Structures and Physical Properties of Rare-Earth Chromium Germanides $RECrGe_3$ (RE = La−Nd, Sm)

Haiying Bie,[†] Oksana Ya. Zelinska,[†,‡] Andriy V. Tkachuk,[†] and Arthur Mar*[,†]

Department of Chemistry, University of Alberta, Edmonton, Alberta, Canada T6G 2G2, and Department of Inorganic Chemistry, Ivan Franko National University of Lviv, 79005 Lviv, Ukraine

Received May 10, 2007. Revised Manuscript Received June 28, 2007

The ternary rare-earth chromium germanides $RECrGe_3$ (RE = La−Nd, Sm) have been synthesized by direct reactions of the elements in the presence of Sn flux, or by arc-melting and annealing at 800 °C. Their structures were determined by single-crystal and powder X-ray diffraction. They adopt a hexagonal perovskite structure type ($P6_3/mmc$, $Z = 2$; $a = 6.2004(1)-6.0812(3)$ Å, $c = 5.7660(6)-5.6594(3)$ Å for RE = La−Sm), unusual for an intermetallic compound, in which chains of face-sharing Cr-centered octahedra are linked by triangular Ge_3 clusters. Electrical resistivity measurements show metallic behavior for all RE members, with prominent transitions that coincide closely with ferromagnetic transitions (T_c ranging from 60 to 155 K) seen in the magnetic susceptibility curves. Band structure calculations on $LaCrGe_3$ show the presence of a narrow, partially filled band with high DOS at the Fermi level.

Introduction

The wide variety of magnetic properties displayed by intermetallic compounds containing rare-earth (RE) and transition metals (M) arises from differing interactions between the localized f-electrons of the RE atoms, through the possible intermediary of the d-electrons of the M atoms. Our own work on ternary rare-earth transition-metal antimonides has revealed compounds such as $RECrSb_3$ that exhibit magnetic ordering.[1] Because Ge and Sb have similar electronegativities and atomic radii, exemplifying what might be regarded as a diagonal relationship in the periodic table, we were interested in extending this work to ternary germanides. Numerous ternary RE−M−Ge phases have now been identified, especially with the later transition metals from the Fe, Co, Ni, and Cu triads; in contrast, much less is known about those containing an early transition metal.[2] In the RE−(Ti, V, or Cr)−Ge systems, the only known phases so far are $RETiGe$,[3−7] $RETiGe_3$,[8,9] $RE_2Ti_3Ge_4$,[10−12] $Sc_xV_{5-x}Ge_3$,[13] $Sc_2V_3Ge_4$,[14,15] $Sc_{1+x}V_{5-x}Ge_5$,[15] $Sc_2Cr_4Ge_5$,[16] $Sc_7Cr_{4+x}Ge_{10-x}$,[16,17] $ScCrGe_2$,[16] La_5CrGe_3,[18] $Nd_2Cr_9Ge_8$,[19] $Sm_{117}Cr_{52}Ge_{112}$,[20] and $RECr_6Ge_6$.[21,22] Among these phases, $RETiGe_3$ (RE = La, Ce, Pr)[9] is worthy of attention because it represents an unusual example of an intermetallic phase adopting the hexagonal perovskite structure type,[23] which consists of one-dimensional chains of face-sharing octahedra and is normally found for chalcogenides and halides. $CeTiGe_3$ was shown to order ferromagnetically with a low Curie temperature (T_c) of 14 K and was proposed to be a dense Kondo lattice compound.[9]

We report here the new series $RECrGe_3$ (RE = La−Nd, Sm) also adopting the hexagonal perovskite structure type. These compounds are also ferromagnetic, but the substitution of Cr for Ti increases the ordering temperatures significantly in $RECrGe_3$ because of magnetic interactions involving the Cr moments.

Experimental Section

Synthesis. Starting materials were RE pieces (99.9%, Hefa), Cr powder (99.8%, Alfa-Aesar), and Ge powder (99.999%, Cerac).

* To whom correspondence should be addressed. E-mail: arthur.mar@ualberta.ca.

[†] University of Alberta.

[‡] Ivan Franko National University of Lviv.

(1) Crerar, S. J.; Deakin, L.; Mar, A. *Chem. Mater.* **2005**, *17*, 2780−2784 and references therein.
(2) Salamakha, P. S.; Sologub, O. L.; Bodak, O. I. In *Handbook on the Physics and Chemistry of Rare Earths*; Gschneidner, K. A., Jr., Eyring, L., Eds.; Elsevier: Amsterdam, 1999; Vol. 27, pp 1−223.
(3) Morozkin, A. V.; Seropegin, Yu. D.; Leonov, A. V.; Sviridov, I. A.; Tskhadadze, I. A.; Nikitin, S. A. *J. Alloys Compd.* **1998**, *267*, L14−L15.
(4) Nikitin, S. A.; Tskhadadze, I. A.; Telegina, I. V.; Morozkin, A. V.; Seropegin, Yu. D. *J. Magn. Magn. Mater.* **1998**, *182*, 375−380.
(5) Welter, R.; Vernière, A.; Venturini, G.; Malaman, B. *J. Alloys Compd.* **1999**, *283*, 54−58.
(6) Morozkin, A. V.; Seropegin, Yu. D.; Sviridov, I. A. *J. Alloys Compd.* **1999**, *285*, L5−L7.
(7) Vernière, A.; Klosek, V.; Welter, R.; Venturini, G.; Isnard, O.; Malaman, B. *J. Magn. Magn. Mater.* **2001**, *234*, 261−273.
(8) Morozkin, A. V. *J. Alloys Compd.* **2004**, *370*, L1−L3.
(9) Manfrinetti, P.; Dhar, S. K.; Kulkarni, R.; Morozkin, A. V. *Solid State Commun.* **2005**, *135*, 444−448.
(10) Morozkin, A. V.; Seropegin, Yu. D.; Portnoy, V. K.; Leonov, A. V.; Sviridov, I. A. *J. Alloys Compd.* **1998**, *278*, L8−L9.
(11) Morozkin, A. V. *J. Alloys Compd.* **1999**, *287*, 185−188.
(12) Nirmala, R.; Sankaranarayanan, V.; Sethupathi, K.; Rangarajan, G.; Morozkin, A. V.; Kundaliya, D. C.; Malik, S. K. *J. Appl. Phys.* **2004**, *95*, 7079−7081.
(13) Kotur, B. Ya.; Bodak, O. I.; Sikiritsa, M.; Bruvo, M. *Dopov. Akad. Nauk Ukr. RSR, Ser. B* **1983**, (*10*), 46−49.
(14) Kotur, B. Ya.; Bodak, O. I.; Zavodnik, V. E. *Sov. Phys. Crystallogr.* **1986**, *31*, 513−516 (*Transl. Kristallografiya* **1986**, *31*, 868−873).
(15) Kotur, B. Ya. *Inorg. Mater.* **1987**, *23*, 493−496 (*Transl. Izv. Akad. Nauk SSSR, Neorg. Mater.* **1987**, *23*, 558−561).
(16) Kotur, B. Ya.; Kravs, A. B.; Andrusyak, R. I. *Russ. Metall.* **1988**, (*6*), 192−195 (*Transl. Izv. Akad. Nauk SSSR, Metally* **1988**, (*6*), 198−201).
(17) Kotur, B. Ya.; Andrusyak, R. I.; Zavodnik, V. E. *Sov. Phys. Crystallogr.* **1988**, *33*, 141−142 (*Transl. Kristallografiya* **1988**, *33*, 240−241).
(18) Guloy, A. M.; Corbett, J. D. *Inorg. Chem.* **1993**, *32*, 3532−3540.
(19) Bodak, O. I.; Gladyshevskii, E. I.; Salamakha, P. S.; Pecharskii, V. K.; Bruskov, V. A. *Sov. Phys. Crystallogr.* **1989**, *34*, 774−775 (*Transl. Kristallografiya* **1989**, *34*, 1285−1287).
(20) Morozkin, A. V.; Seropegin, Yu. D.; Portnoy, V. K.; Sviridov, I. A.; Leonov, A. V. *Mater. Res. Bull.* **1998**, *33*, 903−908.
(21) Brabers, J. H. V. J.; Buschow, K. H. J.; de Boer, F. R. *J. Alloys Compd.* **1994**, *205*, 77−80.
(22) Schobinger-Papamantellos, P.; Rodríguez-Carvajal, J.; Buschow, K. H. J. *J. Alloys Compd.* **1997**, *256*, 92−96.
(23) Müller, U. *Inorganic Structural Chemistry*; Wiley: Chichester, U.K., 1993.

10.1021/cm071276+ CCC: $37.00
Published on Web 08/15/2007

Table 1. Crystallographic Data for $RECrGe_3$ (RE = La−Nd, Sm)

	$LaCrGe_3$	$CeCrGe_3$	$PrCrGe_3$	$NdCrGe_3$	$SmCrGe_3$
formula mass	408.68	409.89	410.68	414.01	420.11
space group	$P6_3/mmc$ (No. 194)	$P6_3/mmc$ (No. 194)	$P6_3/mmc$ (No. 194)	$P6_3/mmc$ (No. 194)	$P6_3/mmc$ (No. 194)
a (Å)	6.2004(7)	6.150(2)	6.1416(6)	6.1264(4)	6.0812(3)
c (Å)	5.7660(6)	5.7222(19)	5.7039(5)	5.6914(4)	5.6594(3)
V (Å^3)	191.97(4)	187.45(11)	186.32(3)	185.00(2)	181.25(2)
Z	2	2	2	2	2
ρ_{calcd} (g cm^{-3})	7.070	7.262	7.320	7.432	7.694
radiation, λ (Å)	Mo $K\alpha$, 0.71073	Mo $K\alpha$, 0.71073	Mo $K\alpha$, 0.71073	Mo $K\alpha$, 0.71073	Cu $K\alpha_1$, 1.54056
μ (mm^{-1})	36.59	38.22	39.31	40.46	169.79
2θ range (deg)	7.58−66.08	7.66−66.20	7.66−66.02	7.68−52.68	10.00−100.00
no. of data collected	2235 (R_{int} = 0.055)	2237 (R_{int} = 0.051)	2191 (R_{int} = 0.049)	1395 (R_{int} = 0.047)	3103 data points
no. of unique data (no. with $F^2 > 2\sigma(F^2)$)	165 (159)	161 (161)	160 (160)	93 (93)	49 Bragg reflns
no. of variables	10	10	10	10	19
residuals[a]	$R(F)(F^2 > 2\sigma(F^2))$ = 0.024 $R_w(F^2)$ = 0.052	$R(F)(F^2 > 2\sigma(F^2))$ = 0.028 $R_w(F^2)$ = 0.070	$R(F)(F^2 > 2\sigma(F^2))$ = 0.032 $R_w(F^2)$ = 0.075	$R(F)(F^2 > 2\sigma(F^2))$ = 0.024 $R_w(F^2)$ = 0.064	R_B = 0.050, R_p = 0.046 R_{wp} = 0.065
GOF	1.299	1.079	1.334	1.064	2.56

[a] $R_B = \sum|I_o - I_c|/\sum I_o$; $R_p = \sum|y_o - y_c|/\sum y_o$; $R_{wp} = [\sum[w(y_o - y_c)]/\sum w y_o^2]^{1/2}$; $R(F) = \sum||F_o| - |F_c||/\sum|F_o|$; $R_w(F_o^2) = [\sum[w(F_o^2 - F_c^2)^2]/\sum wF_o^4]^{1/2}$, $w^{-1} = [\sigma^2(F_o^2) + (Ap)^2 + Bp]$ where $p = [\max(F_o^2,0) + 2F_c^2]/3$.

Single crystals of $RECrGe_3$ used for structure determination were grown from mixtures of RE, Cr, Ge, and Sn in the molar ratio 3:1:5:10, contained in alumina crucibles placed within sealed and evacuated fused-silica tubes. The presence of excess Sn, which acts as a flux, aids in improving crystal quality. The samples were heated at 850 °C for 4 days, heated at 500 °C for 4 days, and then cooled to room temperature over the course of 1 day. After treatment with 6 M HCl to dissolve the Sn flux, needle-shaped crystals of $RECrGe_3$ could be obtained for RE = La−Nd, with typical lengths of up to ∼0.5 mm. Energy-dispersive X-ray (EDX) analysis with a Hitachi S-2700 scanning electron microscope on these crystals showed the presence of all three elements in ratios (18−22% RE, 17−25% Cr, 56−61% Ge) that are consistent with the formulas obtained from the structure determinations.

Powder samples of $RECrGe_3$ (RE = La−Nd, Sm) could be obtained by arc melting of stoichiometric mixtures of the elements in the form of pieces or rods (99.9% or better). The mixtures were melted twice under an argon atmosphere in an Edmund Bühler MAM-1 compact arc melter. The arc-melted ingots were then sealed in evacuated fused-silica tubes and annealed at 800 °C for 20 days, followed by being quenched in cold water. Powder X-ray diffraction patterns of the arc-melted samples, obtained on an Inel powder diffractometer (Cu $K\alpha_1$ radiation) equipped with a CPS 120 detector, were in good agreement with those calculated from the single-crystal data. The samples were phase-pure, except for that with RE = Sm, which contained a small amount of Ge (∼8%) and presumably other undisclosed binary phases in addition to $SmCrGe_3$.

Attempts were made to extend the $RECrGe_3$ series to other RE members. Our investigations revealed that the $RECrGe_3$ phase could not be formed for RE = Gd−Yb at 800 °C.

Structure Determination. Single-crystal intensity data for $RECrGe_3$ (RE = La−Nd) were collected on a Bruker Platform/SMART 1000 CCD diffractometer at 22 °C using ω scans. Structure solution and refinement were carried out with use of the SHELXTL (version 6.12) program package.[24] Face-indexed numerical absorption corrections were applied. Laue symmetry and systematic absences were consistent with the hexagonal space groups $P6_3mc$, $P62c$, and $P6_3/mmc$. The centrosymmetric space group $P6_3/mmc$ was chosen and initial atomic positions were found by direct methods. Refinements proceeded in a straightforward manner. Refinements on the occupancy factors confirmed that all sites are fully occupied with reasonable displacement parameters. Atomic positions were standardized with the program STRUCTURE TIDY.[25] Further data, in the form of a crystallographic information file (CIF), are available as Supporting Information or may be obtained from Fachinformationszentrum Karlsruhe, Abt. PROKA, 76344 Eggenstein-Leopoldshafen, Germany (No. CSD-418424 ($LaCrGe_3$), 418425 ($CeCrGe_3$), 418426 ($PrCrGe_3$), 418427 ($NdCrGe_3$)).

Table 2. Positional and Equivalent Isotropic Displacement Parameters (Å^2) for $RECrGe_3$ (RE = La−Nd, Sm)[a]

	$LaCrGe_3$	$CeCrGe_3$	$PrCrGe_3$	$NdCrGe_3$	$SmCrGe_3$
RE at 2*d* (1/3, 2/3, 3/4)					
U_{eq}	0.0082(3)	0.0099(4)	0.0063(4)	0.0101(6)	0.006(1)
Cr at 2*a* (0, 0, 0)					
U_{eq}	0.0077(4)	0.0094(5)	0.0052(5)	0.0096(8)	0.013(3)
Ge at 6*h* (*x*, 2*x*, 1/4)					
x	0.1934(1)	0.1931(1)	0.1934(1)	0.1932(2)	0.1889(3)
U_{eq}	0.0078(3)	0.0104(4)	0.0063(4)	0.0101(6)	0.002(1)

[a] U_{eq} is defined as one-third of the trace of the orthogonalized U_{ij} tensor. U_{iso} applies to $SmCrGe_3$.

Table 3. Selected Interatomic Distances (Å) in $RECrGe_3$ (RE = La−Nd, Sm)

	$LaCrGe_3$	$CeCrGe_3$	$PrCrGe_3$	$NdCrGe_3$	$SmCrGe_3$
RE−Ge (×6)	3.1134(4)	3.0880(11)	3.0839(3)	3.0761(2)	3.0496(3)
RE−Ge (×6)	3.2514(5)	3.2277(10)	3.2173(5)	3.2107(7)	3.213(2)
Cr−Ge (×6)	2.5278(7)	2.5054(11)	2.5027(9)	2.4957(13)	2.442(3)
Cr−Cr (×2)	2.8830(3)	2.8611(9)	2.8519(3)	2.8457(2)	2.8297(1)
Ge−Ge (×2)	2.6038(14)	2.588(2)	2.5792(18)	2.575(3)	2.635(6)

Powder X-ray diffraction data collected for $RECrGe_3$ (RE = La−Nd, Sm) were also refined with the full-profile Rietveld method using the program LHPM-Rietica.[26] Initial positions were taken from the single-crystal structures determined above. The final cycle of least-squares refinement included scale factor, background, zero point, cell parameters, pseudo-Voigt peak profile parameters, atomic coordinates, and isotropic displacement parameters. Fits to the powder patterns are shown in Figure S1 and the Rietveld refinement results are summarized in Table S1 of the Supporting Information.

Crystal data from the single-crystal structure determinations of $RECrGe_3$ (RE = La−Nd) and the Rietveld refinement of $SmCrGe_3$ are given in Table 1. Final values of the positional and displacement parameters are given in Table 2. Interatomic distances are listed in Table 3.

Electrical and Magnetic Properties. Electrical resistivities from 2 to 300 K were measured on needle-shaped single crystals of $RECrGe_3$ (RE = La−Nd) that had been used for the single-crystal structure determinations by standard four-probe techniques on a Quantum Design PPMS system equipped with an ac transport

(24) Sheldrick, G. M. *SHELXTL*, version 6.12; Bruker AXS: Madison, WI, 2001.
(25) Gelato, L. M.; Parthé, E. *J. Appl. Crystallogr.* **1987**, *20*, 139−143.
(26) Hunter, B. *LHPM-Rietica*, version 1.7.7; International Union of Crystallography Commission on Powder Diffraction Newsletter, 1998, no. 20; www.rietica.org.

controller (model 7100). The current was 100 μA and the frequency was 16 Hz. Given the habit of the crystals, the resistivity could be easily measured only along the needle axis, which corresponds to the crystallographic *c*-axis. All measurements were repeated at least twice.

Measurements of dc magnetic susceptibility were made on powders of RECrGe$_3$ (RE = La−Nd, Sm) between 2 and 300 K on a Quantum Design 9T−PPMS dc magnetometer/ac susceptometer. Susceptibility values were corrected for contributions from the holder and sample diamagnetism. Measurements of ac magnetic susceptibility were made with a driving amplitude of 1 Oe and frequencies between 1000 and 5000 Hz.

Band Structure. Tight-binding linear muffin tin orbital (TB-LMTO) band structure calculations were performed on LaCrGe$_3$ within the local density and atomic spheres approximations using the Stuttgart TB-LMTO program.[27] The basis sets consisted of La 6s, 6p, 5d, 4f; Cr 4s, 4p, 3d; and Ge 4s, 4p, 4d orbitals, with the La 6p and Ge 4d orbitals being downfolded. Integrations in reciprocal space were carried out with an improved tetrahedron method over 95 independent *k* points within the first Brillouin zone. Non-spin-polarized and spin-polarized calculations were carried out.

Results and Discussion

Crystal Structure. The RECrGe$_3$ series forms for the early rare-earths (RE = La−Nd, Sm) and is the most Ge-rich phase found in the RE−Cr−Ge systems so far. The structure consists of chains of face-sharing Cr-centered octahedra, $^1_\infty$[CrGe$_{6/2}$], aligned along the *c* direction, separated by RE atoms (Figure 1). The RE atoms are coordinated by 12 Ge atoms in an anticuboctahedral geometry (Figure 2). On progressing from the La to the Sm member, the RE−Ge distances generally decrease regularly from 3.1134(4) Å (around the planar hexagonal waist) and 3.2514(5) Å (in a trigonal prism) to 3.0496(3) and 3.213(2) Å because of the lanthanide contraction. The surprisingly variable Cr−Ge distances within the Cr-centered octahedra range from 2.5278(7) Å for LaCrGe$_3$ to 2.442(3) Å for SmCrGe$_3$, in good agreement with distances found in Cr$_{11}$Ge$_8$ and Cr$_{11}$Ge$_{19}$[28,29] and slightly longer than the sum of the single-bond metallic radii (Cr, 1.186 Å; Ge, 1.242 Å).[30] Face-sharing of octahedra is normally disfavored in solid-state structures because of the repulsions experienced by cationic centers in close proximity, unless charges are small or another overriding factor such as metal−metal bonding is present. Both effects are probably occurring in RECrGe$_3$, where the Cr−Cr distances along the face-sharing octahedral chains (2.8830(3)−2.8297(1) Å) are suggestive of weak metal−metal bonding. Despite the appearance of a one-dimensional structure, an interesting feature is that these chains are linked by Ge−Ge interactions in the form of triangular clusters so that strong bonding really extends in all three dimensions in the structure (Figure 1). Consistent with single bonds, these Ge−Ge distances are quite short (2.6038(14)−2.575(3) Å),

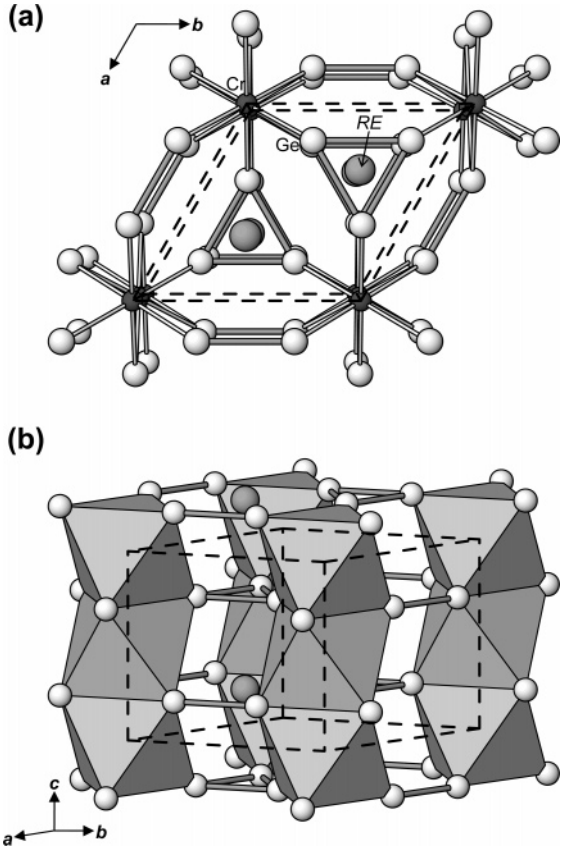

Figure 1. Structure of RECrGe$_3$ (RE = La−Nd, Sm) viewed (a) down the *c*-direction in a ball-and-stick representation and (b) perpendicular to the *c*-direction in a polyhedral representation.

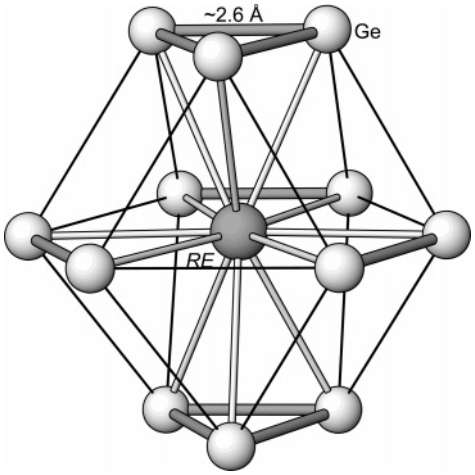

Figure 2. Anticuboctahedral coordination of Ge atoms around the RE center in RECrGe$_3$.

slightly longer than those in the covalently bonded Ge−Ge dimers in Gd$_2$MgGe$_2$ (2.525(3) Å),[31] and relatively invariant with RE substitution.

The structure of RECrGe$_3$ can be identified as a hexagonal perovskite (BaNiO$_3$-type or BaVS$_3$-type),[32,33] which is more commonly adopted by chalcogenides ABQ$_3$ and halides ABX$_3$. This and the isostructural RETiGe$_3$ series[9] are the

(27) Tank, R.; Jepsen, O.; Burkhardt, A.; Andersen, O. K. *TB−LMTO−ASA Program*, version 4.7; Max Planck Institut für Festkörperforschung: Stuttgart, Germany, 1998.
(28) Israiloff, P.; Völlenkle, H.; Wittmann, A. *Monatsh. Chem.* **1974**, *105*, 1387−1404.
(29) Völlenkle, H.; Preisinger, A.; Nowotny, H.; Wittmann, A. *Z. Kristallogr.* **1967**, *124*, 9−25.
(30) Pauling, L. *The Nature of the Chemical Bond*, 3rd ed.; Cornell University Press: Ithaca, NY, 1960.
(31) Choe, W.; Miller, G. J.; Levin, E. M. *J. Alloys Compd.* **2001**, *329*, 121−130.
(32) Takeda, Y.; Kanamaru, F.; Shimada, M.; Koizumi, M. *Acta Crystallogr., Sect. B* **1976**, *32*, 2464−2466.
(33) Gardner, R. A.; Vlasse, M.; Wold, A. *Acta Crystallogr., Sect. B* **1969**, *25*, 781−787.

Table 4. Summary of Resistivity and Magnetism Data for $RECrGe_3$ (RE = La−Nd, Sm)

	$LaCrGe_3$	$CeCrGe_3$	$PrCrGe_3$	$NdCrGe_3$	$SmCrGe_3$
ρ_{300K} ($\mu\Omega$ cm)	410	1020	330	400	
ρ_{2K} ($\mu\Omega$ cm)	75	910	130	110	
ρ_{300K}/ρ_{2K}	5.5	1.1	2.5	3.6	
T_c (K) from:					
ρ vs T plot	80	70	90	103	155
$d(\chi T)/dT$ vs T plot	78	66	97	122	155
χ'_{ac} vs T plot	78	62	92	123	
χ_o (emu/mol)	3.0×10^{-5}	3.2×10^{-4}	7.2×10^{-4}	1.0×10^{-3}	4.6×10^{-4}
θ_p (K)	95	86	110	134	157
μ_{eff} (μ_B/f.u.)	1.4	1.7	2.1	1.8	1.1

only examples known so far of an intermetallic representative of a hexagonal perovskite. Whereas isolated Q^{2-} or X^{1-} species can be regarded to be present in the more ionic representatives, the same cannot be said for $REMGe_3$ (M = Ti, Cr), which must necessarily have a polyanionic substructure. If charges of RE^{3+} and Cr^{3+} are assumed in $RECrGe_3$ in a Zintl-type formalism, the electron transfer to the anionic framework is insufficient to provide each Ge atom with an octet. A hypothetical Ge^{2-} species would then require formation of two additional homoatomic Ge−Ge bonds per atom, on average, to satisfy the octet rule. Although the degree of charge transfer in $REMGe_3$ is expected to be much less pronounced and the notion of localized electrons is questionable, this Zintl-type formalism provides, surprisingly, a satisfying rationalization for the occurrence of triangular Ge_3 clusters, consistent with this prediction of two-bonded Ge atoms.

Properties. Interesting magnetic properties may be anticipated by the presence of Cr atoms in chains, which could interact via intervening RE atoms. Moreover, given the quasi-one-dimensional structure, these properties may be expected to exhibit a high anisotropy. As an initial study of the bulk properties of these $RECrGe_3$ materials, the following magnetic results pertain to powder samples only, whereas electrical resistivities have been measured for single crystals along the *c* direction. Table 4 summarizes the magnetic and electrical data.

$LaCrGe_3$. The electrical resistivity falls linearly with decreasing temperature, characteristic of normal metallic behavior, but at ~80 K, it abruptly drops and then levels off to a residual value of 75 $\mu\Omega$ cm at 2 K (Figure 3a). Correspondingly, the dc magnetic susceptibility increases rapidly below a similar transition temperature, with the zero-field-cooled (zfc) and field-cooled (fc) curves diverging below this point (Figure 3b) because of magnetic domain effects. These observations clearly indicate ferromagnetic behavior, below a Curie temperature of $T_c = 78$ K, as located more precisely from plots of $d(\chi T)/dT$ vs T (not shown) or χ'_{ac} vs T (see the Supporting Information). There appears to be a low-temperature downturn in the susceptibility near ~10 K of uncertain origin. The isothermal magnetization curve at 300 K increases linearly with field, consistent with paramagnetic behavior above T_c (Figure 3c). On the other hand, at 2 K, the magnetization saturates very quickly to $M_s = 0.9$ μ_B/f.u., with little hysteresis as seen by the small remanent magnetization of $M_{rem} = 0.1$ μ_B/f.u., consistent with soft ferromagnetic behavior below T_c. The inverse susceptibility in the high-temperature regime was fit to the modified

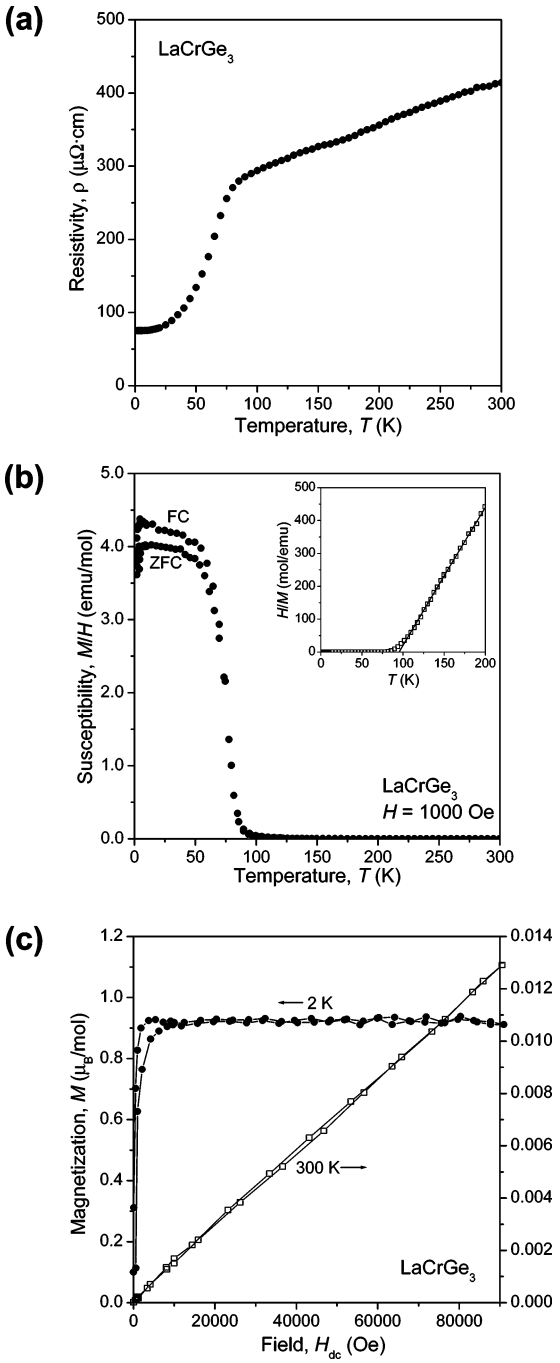

Figure 3. $LaCrGe_3$: (a) electrical resistivity, (b) field-cooled (fc) and zero-field-cooled (zfc) dc magnetic susceptibility (inset, inverse susceptibility plot), and (c) isothermal magnetization at 2 and 300 K.

Curie−Weiss law, $\chi = C/(T - \theta_p) + \chi_o$ (inset of Figure 3b), giving a positive Weiss parameter of $\theta_p = 95$ K, implying ferromagnetic coupling, and a modest temperature-independent term of $\chi_o = 3.0 \times 10^{-5}$ emu/mol. The effective magnetic moment calculated from the Curie constant is 1.4 μ_B/f.u.. Because trivalent La provides no f-electrons, the magnetic moment can be attributed solely to the d-electrons of the Cr atoms. However, this value is significantly lower than would be expected on the basis of Cr^{4+} (2.8 μ_B) or Cr^{3+} ions (3.8 μ_B), clearly in repudiation of a local moment picture for the Cr atoms. These observations for $LaCrGe_3$ are similar to those reported previously for $LaCrSb_3$, which was identified to be a band ferromagnet with $T_c \approx 125$ K and which

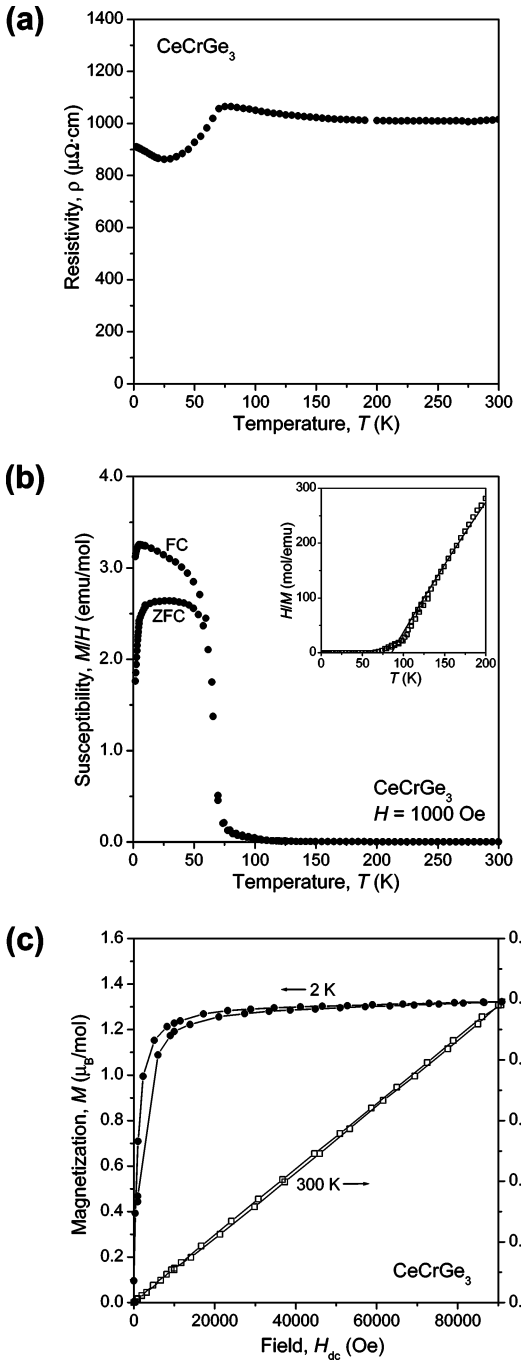

Figure 4. $CeCrGe_3$: (a) electrical resistivity, (b) field-cooled (fc) and zero-field-cooled (zfc) dc magnetic susceptibility (inset, inverse susceptibility plot), and (c) isothermal magnetization at 2 and 300 K.

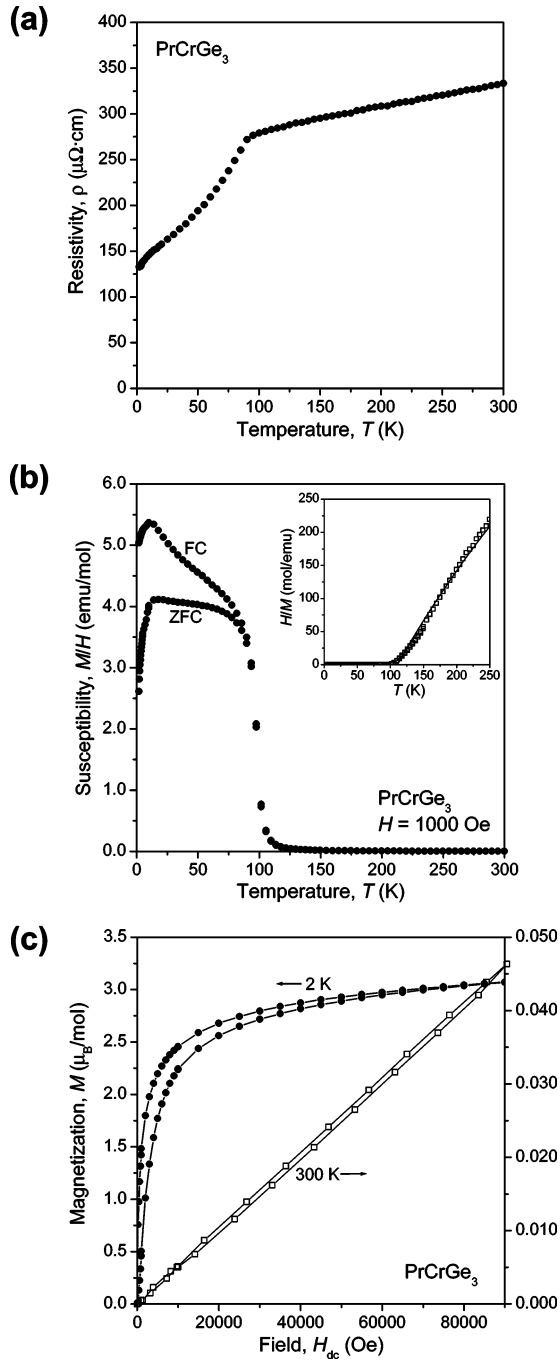

Figure 5. $PrCrGe_3$: (a) electrical resistivity, (b) field-cooled (fc) and zero-field-cooled (zfc) dc magnetic susceptibility (inset, inverse susceptibility plot), and (c) isothermal magnetization at 2 and 300 K.

also has an apparently depressed Cr moment.[34] Despite their identical chemical formulas and the presence of face-sharing Cr-centered octahedra in both structures, they differ in that the Cr−Cr distances are somewhat longer (3.08 Å) and the chains are connected to form layers in $LaCrSb_3$.[35]

$CeCrGe_3$. The electrical resistivity profile for $CeCrGe_3$ is distinctly different from that of $LaCrGe_3$. With decreasing temperature, the resistivity gradually increases to a maximum at ∼70 K and then falls to a shallow minimum centered around 25 K before rising again to 910 $\mu\Omega$ cm at 2 K (Figure 4a). This profile resembles that found in other Ce-containing intermetallics such as $CeTiGe_3$ (which is isostructural to $CeCrGe_3$),[9] $CePdSb_2$,[36] and $CeAgSb_2$,[36,37] which have been proposed to be dense Kondo lattice compounds, except that the resistivity does not decrease as much in the low-temperature regime in $CeCrGe_3$. The rapid upturn in the dc magnetic susceptibility at a similar temperature (Figure 4b) and the saturation behavior of the isothermal magnetization

(34) Raju, N. P.; Greedan, J. E.; Ferguson, M. J.; Mar, A. *Chem. Mater.* **1998**, *10*, 3630−3635.
(35) Ferguson, M. J.; Hushagen, R. W.; Mar, A. *J. Alloys Compd.* **1997**, *249*, 191−198.
(36) Muro, Y.; Takeda, N.; Ishikawa, M. *J. Alloys Compd.* **1997**, *257*, 23−29.
(37) Jobiliong, E.; Brooks, J. S.; Choi, E. S.; Lee, H.; Fisk, Z. *Phys. Rev. B* **2005**, *72*, 104428-1−104428-9.

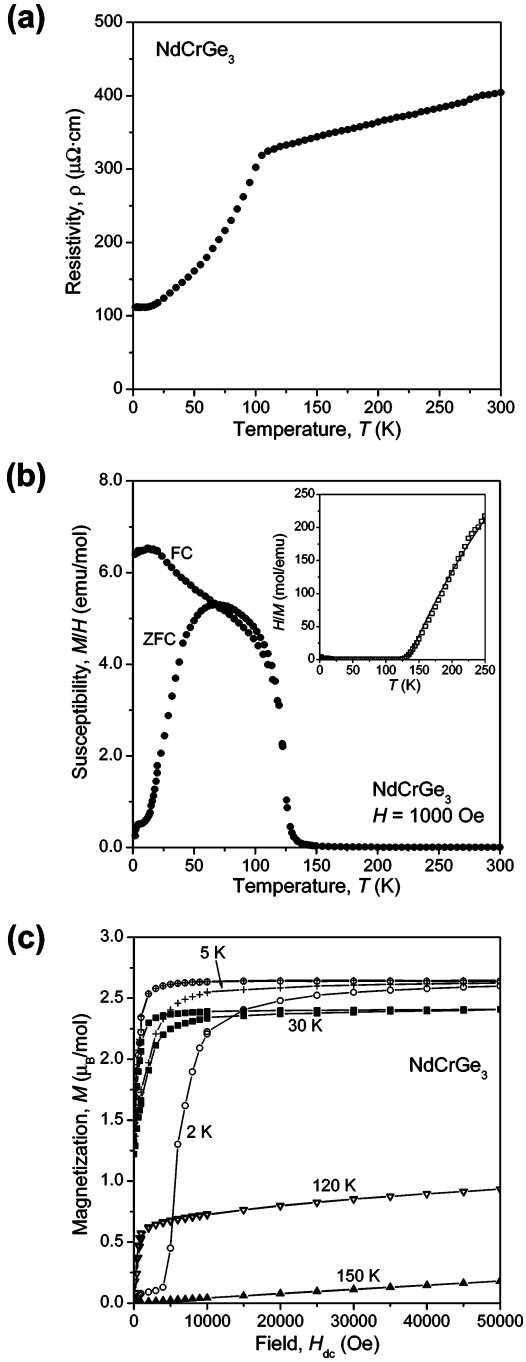

Figure 6. $NdCrGe_3$: (a) electrical resistivity, (b) field-cooled (fc) and zero-field-cooled (zfc) dc magnetic susceptibility (inset, inverse susceptibility plot), and (c) isothermal magnetization at various temperatures.

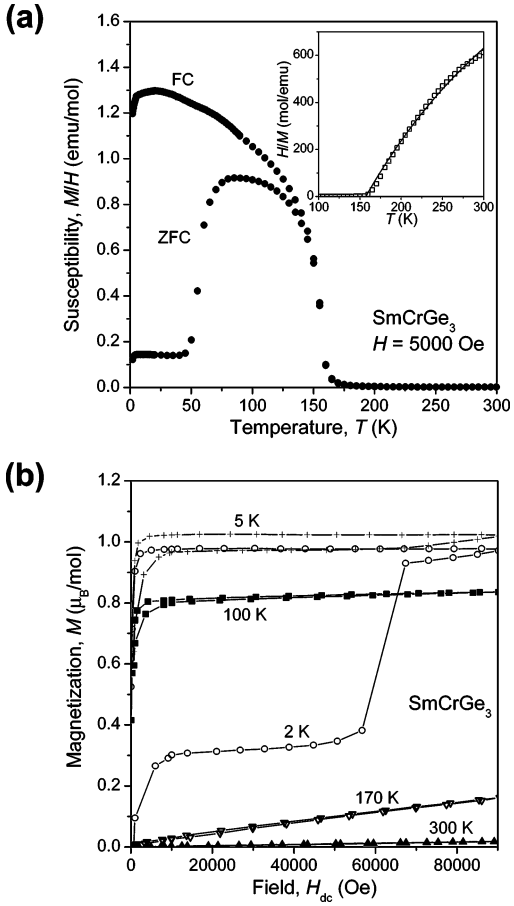

Figure 7. $SmCrGe_3$: (a) field-cooled (fc) and zero-field-cooled (zfc) dc magnetic susceptibility (inset, inverse susceptibility plot), and (b) isothermal magnetization at various temperatures.

at 2 K (Figure 4c) again imply ferromagnetism. The Curie temperature located from $d(\chi T)/dT$ vs T or χ'_{ac} vs T plots is 66 K or 62 K, respectively, slightly lower than the transition temperature in the electrical resistivity curve. Fitting of the high-temperature inverse susceptibility to the modified Curie−Weiss law gave $\theta_p = 86$ K. Interestingly, the effective magnetic moment of 1.7 μ_B/f.u. in $CeCrGe_3$ is not significantly higher than that (1.4 μ_B/f.u.) in $LaCrGe_3$, despite the nominal introduction of a 4f moment, if trivalent cerium is assumed (which has a free-ion moment of 2.5 μ_B). In fact, this value remains less than that (2.6 μ_B/f.u.) in $CeTiGe_3$, which has a much lower ordering temperature ($T_c = 14$ K) and a negative Weiss parameter ($\theta_p = -36$ K).[9] These observations suggest strong interactions of Cr d-moments with the Ce f-moments in $CeCrGe_3$, in a nontrivial arrangement that will need to be determined by further study such as neutron diffraction.

$PrCrGe_3$ and $NdCrGe_3$. The electrical resistivity plots for $PrCrGe_3$ (Figure 5a) and $NdCrGe_3$ (Figure 6a) are similar in profile and absolute values, with sharp transitions at 90 and 103 K, respectively. These transitions coincide with the rapid upturns in the dc magnetic susceptibility, at 97 K (Figure 5b) and 122 K (Figure 6b), respectively. Additional transitions are seen in the susceptibility at low temperatures. In $PrCrGe_3$, all isothermal magnetization curves below T_c exhibit saturation behavior (the 2 K curve is shown in Figure 5c; further curves are in the Supporting Information), with no striking changes seen in their profiles other than the expected increase in saturation magnetization as the temperature is decreased. In $NdCrGe_3$, however, the isothermal magnetization curve at 2 K exhibits strong hysteresis ($M_{rem} = 1.4$ μ_B/f.u.), which becomes less pronounced at higher temperature (Figure 6c). The increasing importance of the role of f-electrons can be surmised from the dramatic low-temperature downturns in the zfc curves of the magnetic susceptibility on progressing from $LaCrGe_3$ to $NdCrGe_3$, which may be related to different degrees of magnetic anisotropy associated with the rare earth. The effective magnetic moment (determined from fits of the high-temperature susceptibility to the modified Curie−Weiss law) also decreases on going from $PrCrGe_3$ (2.1 μ_B/f.u.) to $NdCrGe_3$

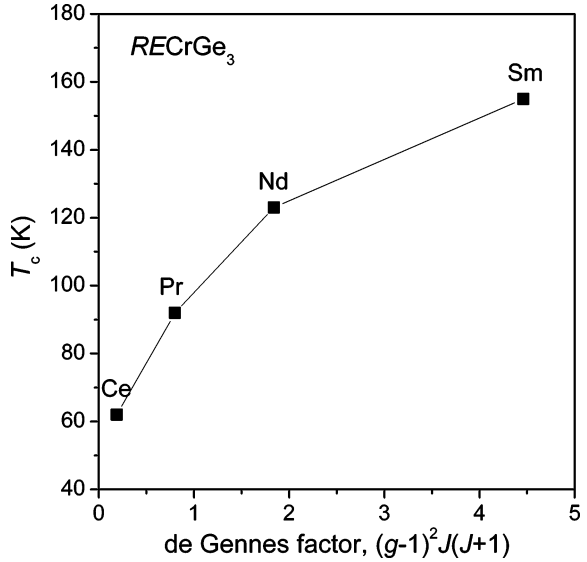

Figure 8. Magnetic ordering temperatures for RECrGe$_3$ plotted versus the de Gennes factor.

(1.8 μ_B/f.u.), suggesting a distinct change in the nature of magnetic interactions between the RE and Cr moments.

SmCrGe$_3$. The resistivity of SmCrGe$_3$ was not measured because of the lack of suitably sized crystals, but it may be predicted to have a similar profile as other RECrGe$_3$ members. Inspection of the dc magnetic susceptibility shows that the Curie temperature is now increased to 155 K (Figure 7a). The low-temperature transition at 55 K becomes quite prominent. Below this transition, the isothermal magnetization at 2 K first appears to saturate at 0.3 μ_B, but then increases abruptly at 60 kOe to saturate again at 1.0 μ_B (Figure 7b). At 5 K, the curve only shows saturation at 1.0 μ_B. These observations suggest the onset of a low-field, low-temperature ferromagnetic phase stable below 5 K and below 60 kOe.

In general, all RECrGe$_3$ compounds studied here are metallic and exhibit a prominent kink in their electrical resistivity curves that is clearly magnetic in origin, as it coincides with a ferromagnetic transition seen in the magnetic susceptibility curves. The sudden decrease in resistivity arises because of a loss of spin-disorder scattering as ferromagnetic ordering sets in. This ferromagnetic ordering arises from interaction between Cr moments, mediated through the RE atoms. The Curie temperatures are found to be roughly proportional to the de Gennes factor, $(g - 1)^2(J(J + 1))$ (Figure 8), implying that the localized 4f electrons on the RE atoms interact indirectly with each other through polarization of the conduction electrons (RKKY interaction). This correlation and the low observed effective magnetic moments also suggest that Cr d electrons are highly delocalized in conduction bands.

Electronic Structure. To gain insight on the bonding and properties of RECrGe$_3$, a band structure calculation was carried out for LaCrGe$_3$. Figure 9 shows the density of states (DOS) curve for LaCrGe$_3$, as well as its contributions from La, Cr, and Ge. In general agreement with the formulation $(La^{3+})(Cr^{3+})(Ge^{2-})_3$ derived from the simple electron counting scheme proposed earlier, most of the La states are unoccupied and located above the Fermi level, whereas the Cr- and Ge-based bands are partially filled. Strong covalent bonding is implied by the mixing of Cr and Ge states over a wide energy range (from −6 eV upward). As seen in the crystal orbital Hamiltonian population (COHP) curves, Cr−Ge bonding within the Cr-centered octahedra is optimized through complete filling of bonding levels, giving an integrated −COHP of 2.2 eV/bond up to the Fermi level, beyond which are only unoccupied antibonding levels (Figure 10a). Occupation of bonding levels at similar energies and nonbonding levels near the Fermi level accounts for the Ge−Ge bonds within the triangular clusters, giving an integrated −COHP of 1.1 eV/bond (Figure 10b). Perhaps the most striking feature of the band structure is the presence of a very large spike in the DOS near the Fermi level, just below a pseudogap. This spike is almost entirely based on Cr d-states (Figure 9c). A partially filled narrow band with high DOS at the Fermi level is one of the characteristic features of a band ferromagnet, consistent with the experimentally observed metallic and ferromagnetic behavior of LaCrGe$_3$. Moreover, inspection of the COHP curve for the Cr−Cr contacts along the face-sharing octahedral chains reveals that, although there is still net metal−metal bonding overall (integrated −COHP of 1.1 eV/bond), the states at the Fermi

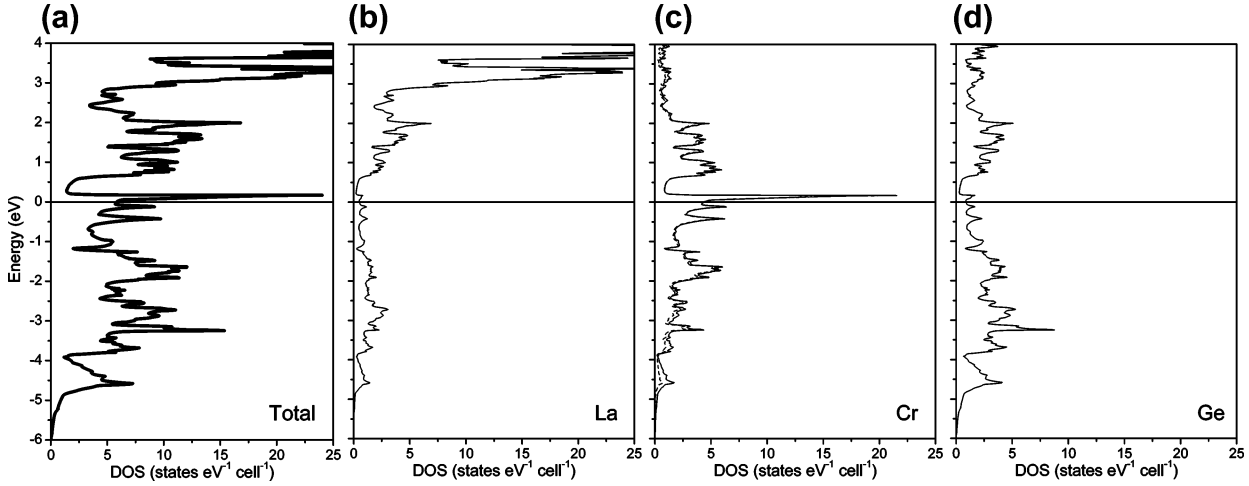

Figure 9. (a) Total density of states (DOS) for non-spin-polarized LaCrGe$_3$ and its (b) La, (c) Cr, and (d) Ge contributions. The dashed curve in (c) indicates the contribution of 3d states to the Cr partial DOS. The Fermi level is marked by a horizontal line at 0 eV.

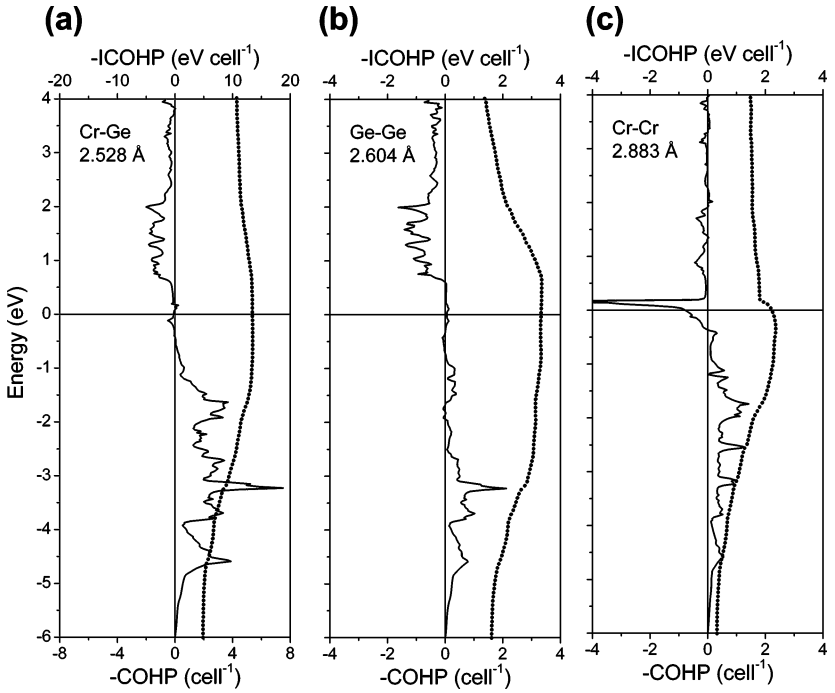

Figure 10. Crystal orbital Hamilton population (COHP) curves (solid line) and integrated COHP curves (dotted line) for (a) Cr−Ge, (b) Ge−Ge, and (c) Cr−Cr contacts in non-spin-polarized $LaCrGe_3$. The Fermi level is marked by a horizontal line at 0 eV.

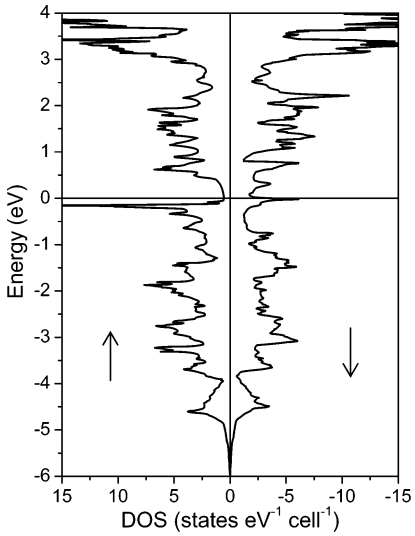

Figure 11. Total density of states for spin-polarized $LaCrGe_3$. The Fermi level is marked by a horizontal line at 0 eV.

level are strongly antibonding (Figure 10c). The electronic instability inherent in this type of situation has been proposed as an alternative way to view the driving force for band ferromagnetism.[38] Figure 11 shows the results of a spin-polarized calculation on $LaCrGe_3$. The DOS curve for the majority spin states (↑) is shifted down relative to that for the minority spin states (↓), with the narrow Cr d band now appearing below the Fermi level. The magnetic state is more stable than the nonmagnetic state by 0.076 eV/cell. The calculated magnetic moment of 1.3 μ_B is derived almost exclusively from Cr 3d states and agrees well with the experimental moment of 1.4 μ_B for $LaCrGe_3$. By extension, we can make the supposition that the Cr d states are also delocalized in narrow d-bands in the other $RECrGe_3$ members to account for the depressed magnetic moments, but the filled RE f-states will also be polarized and contribute to the effective moment.

This investigation has uncovered a new series of intermetallic germanides that have several points of interest: (i) the adoption of a hexagonal perovskite type structure, normally found for halides and chalcogenides, is unusual for an intermetallic compound; (ii) all rare-earth members studied thus far are metallic and ferromagnetic with relatively high transition temperatures; and (iii) more complex magnetic behavior is signalled by other transitions at low temperature or low field. Further work is in progress to examine the RE−Cr−Ge systems systematically to identify other ternary phases, attempt substitutions of Cr with other transition metals, and prepare suitable samples for neutron diffraction measurements. Single-crystal magnetization studies would also be interesting to probe the extent of anisotropy, and optimization of crystal growth is underway.

Acknowledgment. This work was supported by the Natural Sciences and Engineering Research Council of Canada and the University of Alberta. We thank Dr. Robert McDonald and Dr. Michael J. Ferguson (X-ray Crystallography Laboratory) for the X-ray data collection and Ms. Christina Barker (Department of Chemical and Materials Engineering) for assistance with the EDX analysis.

Supporting Information Available: X-ray crystallographic files in CIF format; Rietveld refinement results on powder samples and additional magnetic data (PDF). This material is available free of charge via the Internet at http://pubs.acs.org.

CM071276+

(38) Landrum, G. A.; Dronskowski, R. *Angew. Chem., Int. Ed.* **2000**, *39*, 1560−1585.